Chemical Science

ROYAL SOCIETY OF CHEMISTRY

EDGE ARTICLE

View Article Online
View Journal | View Issue

Cite this: *Chem. Sci.*, 2020, **11**, 4766

All publication charges for this article have been paid for by the Royal Society of Chemistry

Shape-adaptive single-molecule magnetism and hysteresis up to 14 K in oxide clusterfullerenes $Dy_2O@C_{72}$ and $Dy_2O@C_{74}$ with fused pentagon pairs and flexible Dy–(μ_2-O)–Dy angle†

Georgios Velkos, ‡[a] Wei Yang,‡[b] Yang-Rong Yao,[c] Svetlana M. Sudarkova,[ad] XinYe Liu,[b] Bernd Büchner,[a] Stanislav M. Avdoshenko, *[a] Ning Chen *[b] and Alexey A. Popov *[a]

Received 31st January 2020
Accepted 19th April 2020

DOI: 10.1039/d0sc00624f

rsc.li/chemical-science

Dysprosium oxide clusterfullerenes $Dy_2O@C_s(10528)–C_{72}$ and $Dy_2O@C_2(13333)–C_{74}$ are synthesized and characterized by single-crystal X-ray diffraction. Carbon cages of both molecules feature two adjacent pentagon pairs. These pentalene units determine positions of endohedral Dy ions hence the shape of the Dy_2O cluster, which is bent in $Dy_2O@C_{72}$ but linear in $Dy_2O@C_{74}$. Both compounds show slow relaxation of magnetization and magnetic hysteresis. Nearly complete cancelation of ferromagnetic dipolar and antiferromagnetic exchange Dy⋯Dy interactions leads to unusual magnetic properties. $Dy_2O@C_{74}$ exhibits zero-field quantum tunneling of magnetization and magnetic hysteresis up to 14 K, the highest temperature among Dy-clusterfullerenes.

Introduction

Endohedral metallofullerenes (EMFs) comprising metal and non-metal atoms in their endohedral species are known as clusterfullerenes.[1] Enhanced electrostatic interactions between endohedral lanthanides (Ln) and non-metal ions (X^{q-}), such as N^{3-}, S^{2-}, or O^{2-}, reinforced by exceptionally short Ln–X bonds result in a strong magnetic anisotropy of Ln ions and lead to the single-molecule magnetism in many Ln-clusterfullerenes.[2] Especially Dy-clusterfullerenes are known as robust single molecule magnets (SMMs) with many favourable properties, including thermal and chemical stability, reasonably high blocking temperatures of magnetization, and magnetic hysteresis in bulk samples as well as in monolayers on different substrates.[3] Thus, with the improvement of EMF-SMMs, the tremendous progress achieved over the last two decades in the Ln-SMM field[4] has a good chance to further advance to the state of device-oriented functional molecular materials.

Oxide clusterfullerenes[5] with endohedral Ln_2O clusters were predicted to have the largest ligand-field splitting in the whole EMF family[3g,6] and thus are viable synthetic targets as prospective SMM candidates. Indeed, our recent study of three isomers of $Dy_2O@C_{82}$ revealed their unique magnetic properties.[7] The pronounced magnetic anisotropy is combined in these molecules with antiferromagnetic (AFM) exchange interactions, which are the strongest through all dinuclear Dy complexes with non-radical bridging ligands. In this Communication, we report that the encapsulation of the Dy_2O cluster in smaller carbon cages has a profound influence on the magnetic properties and leads to the $Dy_2O@C_{74}$ compound with the highest temperature of magnetic hysteresis among clusterfullerene-SMMs.

Results and discussion

Synthesis, molecular and electronic structure

New Dy-oxide clusterfullerenes $Dy_2O@C_{72}$ and $Dy_2O@C_{74}$ were synthesized by arc-discharge evaporation of Dy_2O_3-filled graphite rods in He/CO_2 atmosphere (200/20 Torr) and isolated by multi-step high-performance liquid chromatography (HPLC) as described in ESI.† Basic characterization of the purified $Dy_2O@C_{72}$ and $Dy_2O@C_{74}$, including their HPLC profiles, high-resolution laser desorption ionization mass spectra with characteristic isotopic patterns, and UV-vis-NIR absorption spectra are surveyed in Fig. 1.

The molecular structures of $Dy_2O@C_{72}$ and $Dy_2O@C_{74}$ were elucidated by single-crystal X-ray diffraction of co-crystals with

[a]*Leibniz Institute for Solid State and Materials Research Helmholtzstraße 20, 01069 Dresden, Germany. E-mail: s.avdoshenko@ifw-dresden.de; a.popov@ifw-dresden.de*
[b]*College of Chemistry, Chemical Engineering and Materials Science, Soochow University, Suzhou, Jiangsu 215123, P.R. China. E-mail: chenning@suda.edu.cn*
[c]*Department of Chemistry, University of Texas at El Paso, 500 W University Avenue, El Paso, Texas 79968, USA*
[d]*Chemistry Department, Moscow State University, 119991 Moscow, Russia*

† Electronic supplementary information (ESI) available. CCDC 1974305 and 1974314. For ESI and crystallographic data in CIF or other electronic format see DOI: 10.1039/d0sc00624f

‡ Equal contribution.

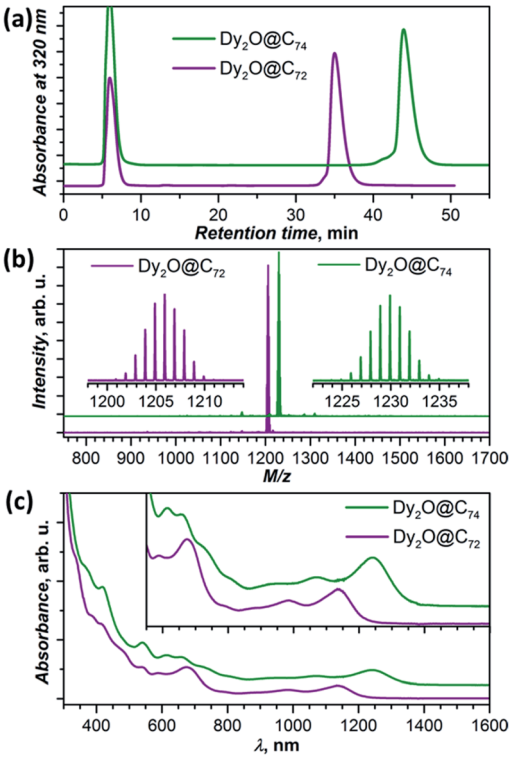

Fig. 1 Characterization of isolated $Dy_2O@C_{72}$ and $Dy_2O@C_{74}$: (a) HPLC profiles (BuckyPrep column, toluene as eluent, flow rate 4 mL min^{-1}; solvent peak appears at 6 min); (b) LDI mass-spectra in a positive-ion mode; (c) UV-Vis-NIR absorption spectra in toluene (the inset shows magnification of the low-energy range).

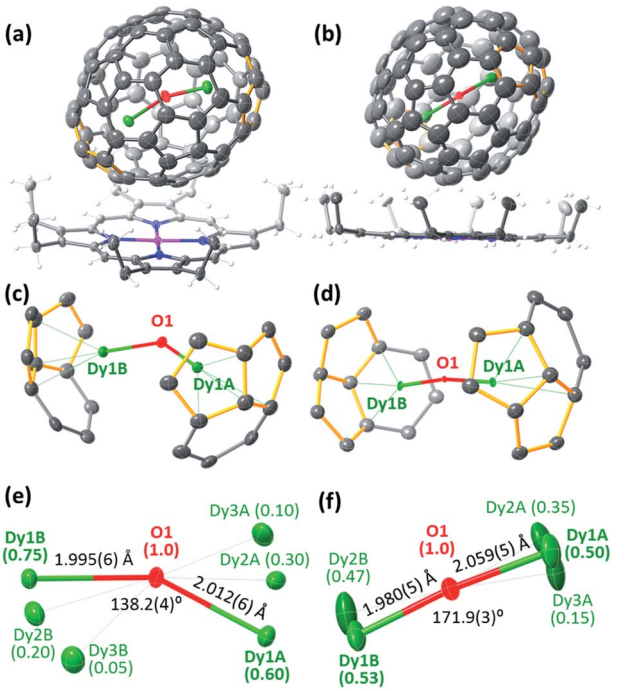

Fig. 2 (a and b) Thermal ellipsoids of $Dy_2O@C_{2n}\cdot Ni^{II}(OEP)$ crystals with 30% probability showing only the major dysprosium sites: (a) $Dy_2O@C_s(10528)–C_{72}$, (b) $Dy_2O@C_2(13333)–C_{74}$; the solvent molecules and minor Dy sites are omitted, Dy is green, O is red, Ni is purple, N is blue, C is grey, adjacent-pentagon pairs are highlighted in orange. (c and d) Interaction of the major Dy_2O site with the closest cage motif in (c) $Dy_2O@C_{72}$, and (d) $Dy_2O@C_{74}$. (e and f) Endohedral Dy_2O units with disordered Dy sites and selected structural parameters in (e) $Dy_2O@C_{72}$, and (f) $Dy_2O@C_{74}$.

$Ni^{II}(OEP)$ revealing $C_s(10528)–C_{72}$ and $C_2(13333)–C_{74}$ carbon cages (Fig. 2a and b).§ Both fullerenes violate the Isolated Pentagon Rule (IPR) and have two pairs of adjacent pentagons, which are stabilized by coordination with Dy ions (Fig. 2c,d). The $C_s(10528)–C_{72}$ cage was found before in $Sc_2S@C_{72}$,[8] $Sc_2C_2@C_{72}$,[9] and presumably $Dy_2S@C_{72}$.[3g] The $C_2(13333)–C_{74}$ cage was predicted theoretically as a plausible isomer of $Sc_2C_2@C_{74}$ [10] and was found recently in $Ho_2O@C_{74}$.[5c]

Carbon cages and oxygen atoms are fully ordered in the crystals, but Dy atoms are less ordered with 2–3 sites for each metal atom (Fig. 2e and f). In $Dy_2O@C_{72}$ the Dy–O–Dy angle is 138.2(4)° for the major Dy sites (occupancy 0.60 and 0.75), whereas in $Dy_2O@C_{74}$ the Dy_2O cluster is close to the linear shape, similar to the Ho_2O cluster in $Ho_2O@C_2(13333)–C_{74}$.[5c] Dy–O bonds are very short, 1.980(5)–2.059(5) Å, but the disorder in Dy positions does not allow detailed analysis. Optimization of the molecular structures performed at the PBE-D level (PAW 4f-in-core potentials, VASP 5.0 code[11]) resulted in the Dy–O distances and Dy–O–Dy angles of 2.025 Å/138° in $Dy_2O@C_{72}$ and 2.038 Å/180° in $Dy_2O@C_{74}$.

Apparently, the variation of the Dy_2O cluster shape from bent to linear is dictated by the Dy···Dy distance, which changes from 3.743(1) Å in $Dy_2O@C_{72}$ to 4.030(2) Å in $Dy_2O@C_{74}$ (DFT values are 3.784 and 4.076 Å, respectively). In due turn, the location of Dy atoms inside the fullerene is determined by the arrangement of pentalene units. The distance between centroids of pentalenes in X-ray structures is 8.151 Å in $Dy_2O@C_{72}$ and 8.597 Å in $Dy_2O@C_{74}$. Thus, the shape of the Dy_2O cluster is imposed by the fullerene cage form-factor.[1c] Note that in $Dy_2O@C_{82}$ isomers the cluster is bent despite the larger cage size than in $Dy_2O@C_{74}$: in fact, Dy···Dy distances in all $Dy_2O@C_{82}$ structures are shorter than in $Dy_2O@C_{74}$.[7] At the same time, the linear shape of the cluster was found in $Ho_2O@D_{2d}(23)–C_{84}$, which also has an elongated shape of the fullerene cage.[5d]

DFT-based molecular dynamics simulations showed that at 300 K on a timescale of 100 ps metal atoms oscillate near their optimized positions (Fig. S4†). IR spectra calculated from the Fourier transform of the time-dependent dipole moment resemble those computed for the static model and agree well with the experimental spectra (Fig. S5†). Antisymmetric Dy–O stretching vibration is found at 680 cm^{-1} in $Dy_2O@C_{72}$ and 700 cm^{-1} in $Dy_2O@C_{74}$.

Electronic absorption spectra of both compounds extend to the near-IR region with the lowest-energy bands at 1137 nm (1.09 eV) in $Dy_2O@C_{72}$ and 1240 nm (1.00 eV) in $Dy_2O@C_{74}$ (Fig. 1c). The spectrum of $Dy_2O@C_{72}$ exhibits a close similarity to the spectra of $Sc_2S@C_{72}$,[8] $Sc_2C_2@C_{72}$,[9] and $Dy_2S@C_{72}$[3g] featuring the same $C_s(10528)–C_{72}$ cage. However, the cluster composition has a noticeable impact on the lowest energy excitation, found at 1076 nm (Sc_2S), 1082 nm (Sc_2C_2), or

Table 1 Redox potentials[a] of $Dy_2O@C_s(10528)-C_{72}$ and $Dy_2O@C_2(13333)-C_{74}$

EMF	O–II	O–I	R–I	R–II	R–III	R–IV	Gap_{EC}
$Dy_2O@C_{72}$	0.87	0.33	−1.09	−1.56	−2.18	−2.55	1.42
$Dy_2O@C_{74}$	1.18	0.52	−0.81	−1.17	−2.16	−2.56	1.33

[a] Measured in $TBAPF_6$/*o*-dichlorobenzene and referred *versus* $Fe(Cp)_2^{+/0}$.

1115 nm (Dy_2S). The absorption spectrum of $Dy_2O@C_{74}$ is virtually identical to that of $Ho_2O@C_2(13333)-C_{74}$.[5c]

Further insight into the electronic structure of Dy_2O clusterfullerenes is obtained from the electrochemical studies. Cyclic voltammograms are shown in Fig. S6† and redox potentials are listed in Table 1. Both $Dy_2O@C_{72}$ and $Dy_2O@C_{74}$ exhibit one reversible oxidation and three reversible reduction steps as well as poorly reversible fourth reduction and second oxidation steps. DFT calculations show that frontier molecular orbitals of both molecules are localized on their fullerene cages (Fig. S7†), which suggests that the redox processes do not affect the Dy_2O cluster. Comparison of the redox potentials of $Dy_2O@C_{72}$ to $Sc_2S@C_{72}$ [8] and $Sc_2C_2@C_{72}$ [9] (Table S2†) reveals that the variation of the optical gap discussed above is also reflected in their electrochemical gaps despite the predominant localization of the frontier MOs on the carbon cage in all molecules.

Magnetic properties

SQUID magnetometry. Magnetic properties of $Dy_2O@C_{72}$ and $Dy_2O@C_{74}$ powders were studied by SQUID magnetometry. Fig. 3a and b show low-temperature magnetization curves measured for two clusterfullerenes with a sweep rate of 2.9 mT s^{-1}. $Dy_2O@C_{72}$ shows open hysteresis up to 7 K (Fig. S8†). In the isostructural $Dy_2S@C_{72}$, the hysteresis is much narrower and is closing already at 3 K.[3g] Thus, once again Dy_2O cluster is found to exhibit more robust single molecule magnetism than the Dy_2S analog with the same fullerene cage. Earlier, superior SMM properties were found for $Dy_2O@C_{82}$ when compared to the isostructural $Dy_2S@C_{82}$.[7] At the same time, the use of softer sulfur co-ligands was found to be beneficial to increase the axiality of other types of single-molecule magnets.[12]

Magnetic hysteresis in $Dy_2O@C_{74}$ closes above 14 K (Fig. S8†). The shape of the hysteresis with the abrupt decay of magnetization near 0 T is different from that of $Dy_2O@C_{72}$ and other dinuclear Dy-clusterfullerenes. Such a "waist-restricted" or "butterfly" hysteresis is characteristic for the quantum tunnelling of magnetization (QTM) in zero field and is common for single-ion magnets, but is not typical for dinuclear SMMs.

Blocking of magnetization is analysed by comparing magnetic susceptibility measured after cooling the sample in zero field (χ_{ZFC}) and during cooling the sample in field (χ_{FC}).[13] Blocking temperature T_B defined as the peak temperature of χ_{ZFC} is near 4 K in $Dy_2O@C_{72}$ and 6.7 K in $Dy_2O@C_{74}$ (Fig. 3) when measured in a field of 0.2 T with the temperature sweep rate of 5 K min^{-1}. However, both fullerenes show bifurcation of χ_{ZFC} and χ_{FC} curves (defined as T_{irrev}[13]) until noticeably higher

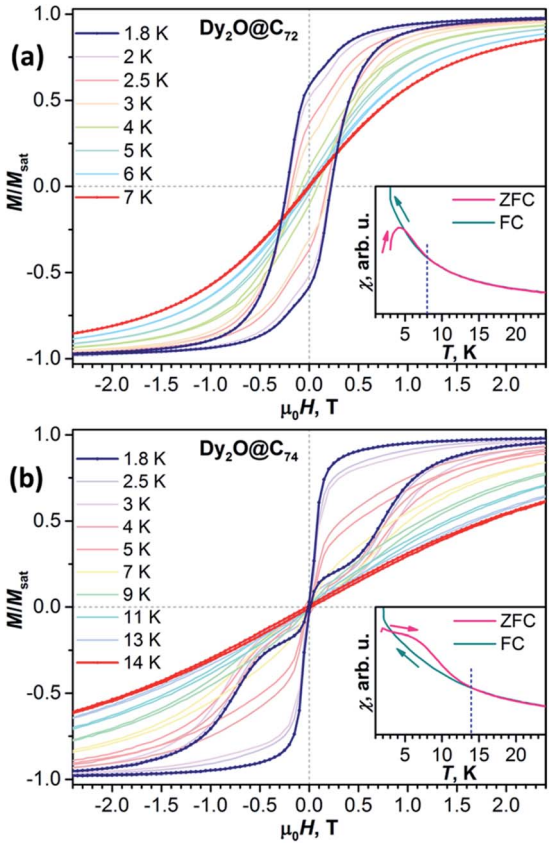

Fig. 3 Magnetic hysteresis curves of $Dy_2O@C_{72}$ (a) and $Dy_2O@C_{74}$ (b) measured with the sweep rate 2.9 mT s^{-1}. Insets show comparison of χ_{FC} and χ_{ZFC} curves ($\mu_0H = 0.2$ T, temperature sweep rate 5 K min^{-1}); dashed blue lines denote T_{irrev} as the temperature, at which χ_{FC} and χ_{ZFC} curves bifurcate.

temperatures, reaching 8 K for $Dy_2O@C_{72}$ and 14 K for $Dy_2O@C_{74}$. The uncommon shape of χ_{ZFC}, being higher than χ_{FC}, is caused in $Dy_2O@C_{74}$ by the fast QTM at small fields. It should be also noted that T_B and T_{irrev} values are kinetic parameters and depend on the magnetic field, sweep rate, and some technical aspects of the measurements (see Fig. S9–S11† for further measurements and ref. 4d for a more detailed discussion). More universal parameter is the temperature T_{B100}, at which relaxation time of magnetization is 100 s. As determined from the relaxation time measurements described below, T_{B100} of $Dy_2O@C_{72}$ is 3.4 K in zero field and 2.6 K at 0.2 T. For $Dy_2O@C_{74}$, the T_{B100} value in zero field is not defined because QTM limits the relaxation time, whereas in the field of 0.2 T the value is 5.0 K.

Relaxation times of magnetization τ_M below T_{irrev} (Tables S3–S8 and Fig. S12†) were determined by the stretched exponential fitting of magnetization decay curves recorded after the fast sweep of the magnetic field from 5 T to a required value. Unfortunately, the isolable amounts of the clusterfullerenes are insufficient for the measurement of relaxation times at higher temperatures by AC magnetometry.

Fig. 4a shows the magnetic field dependence of τ_M measured at a constant temperature. For $Dy_2O@C_{72}$, τ_M decays fast with

the field from 523 s at zero field to 95 s at 0.4 T and then tends to level off. This $\tau_M(H)$ dependence is a clear manifestation of the direct relaxation mechanism. For $Dy_2O@C_{74}$, relaxation rate in 0 T could not be measured because of the fast QTM, and the lowest field studied is 0.05 T. Field dependence at 2.5 K first shows a fast increase of τ_M from 152 s at 0.05 T to 750–780 s at 0.2–0.35 T. This $\tau_M(H)$ dependence corresponds to the gradual quenching of the QTM by increasing Zeeman splitting. With the further field increase beyond 0.35 T, relaxation accelerates due to the contribution of the direct mechanism as in $Dy_2O@C_{72}$.

The temperature dependence of τ_M shown in Fig. 4b cannot be described by a direct process alone. Equally good fits are obtained either for a combination of the direct and Raman mechanisms:

$$\tau_M^{-1}(T) = C_{d,H}T^{n_d} + C_R T^{n_R} \quad (1)$$

or by a combination of the direct and Arrhenius process:

$$\tau_M^{-1}(T) = C_{d,H}T^{n_d} + \tau_0^{-1}\exp(-U^{eff}/T) \quad (2)$$

For the direct mechanism n_d should be 1, and $C_{d,H}$ is field-dependent. For each fullerene, temperature dependence was measured in two different fields (Fig. 4b), and then two datasets were fitted jointly either with eqn (1) or with eqn (2) keeping field-independent parameters identical (Fig. S13 and S14†). Eqn (1) gives more physically sound interpretation of the relaxation of magnetization and will be discussed further. For $Dy_2O@C_{72}$, the procedure returned $n_d = 1.43 \pm 0.13$, $C_{d,0\ T} = (5.2 \pm 0.1)\cdot 10^{-4}\ s^{-1}\ K^{-1.4}$, $C_{d,0.2\ T} = (1.8 \pm 0.2)\cdot 10^{-3}\ s^{-1}\ K^{-1.4}$, $n_R = 3.7 \pm 0.4$, and $C_R = (8 \pm 4)\cdot 10^{-5}\ s^{-1}\ K^{-3.7}$. The n_d value is higher than 1, which may be due to the phonon bottleneck effect (which increases n_d to 2). For $Dy_2O@C_{74}$, we obtained $n_d = 1.23 \pm 0.14$, $C_{d,0.2\ T} = (1.3 \pm 0.3)\cdot 10^{-4}\ s^{-1}\ K^{-1.25}$, $C_{d,0.8\ T} = (4.9 \pm 0.5)\cdot 10^{-4}\ s^{-1}\ K^{-1.25}$, $n_R = 3.28 \pm 0.14$, and $C_R = (4 \pm 1)\cdot 10^{-5}\ s^{-1}\ K^{-3.3}$. For both molecules the direct mechanism dominates at lower temperature and at higher fields, whereas the field-independent Raman process with n_R of 3–4 takes over at higher temperatures.

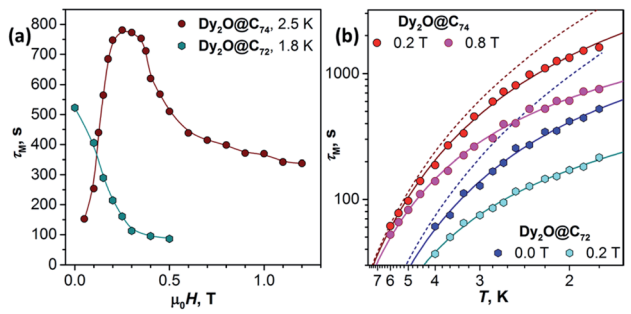

Fig. 4 Magnetization relaxation times of $Dy_2O@C_{72}$ and $Dy_2O@C_{74}$: (a) Field dependence of τ_M at 1.8 K ($Dy_2O@C_{72}$) and 2.5 K ($Dy_2O@C_{74}$). Note that the smallest field for $Dy_2O@C_{74}$ is 0.05 T since the measurements in zero field are not possible because of the fast QTM process; (b) Temperature dependence of τ_M in two different fields, dots are measured values, solid lines are fits by a combination of Raman and direct mechanisms (eqn (1)), dashed lines are contributions of Raman process for $Dy_2O@C_{72}$ (blue) and $Dy_2O@_{74}$ (red).

These relatively small n_R values indicate that optical phonons contribute strongly to the relaxation of magnetization.[14] Contribution of the Raman mechanism is shown for each molecule in Fig. 4b. When eqn (2) was used for the fit, Arrhenius processes with effective barriers of 14–16 K were obtained (see ESI†). These values are much smaller than the ligand-field splitting of Dy^{3+} ions in $Dy_2O@C_{2n}$ molecules, but are considerably larger than the energy difference between the states with ferromagnetic and antiferromagnetic coupling of magnetic moments (see below), and thus cannot match the spin energy levels of the system.

Dy···Dy interactions and magnetic anisotropy. To get better understanding of the Dy···Dy coupling, magnetization curves of $Dy_2O@C_{72,74}$ molecules were simulated and fitted using powder averaging in the PHI code[15] with the following spin Hamiltonian:

$$\hat{H}_{spin} = \hat{H}_{LF_1} + \hat{H}_{LF_2} - 2j_{12}\hat{J}_1\hat{J}_2 + \hat{H}_{ZEE} \quad (3)$$

where $\hat{H}_{LF_i}$ are single-ion ligand-field Hamiltonians of Dy^{3+} with *ab initio* computed parameters, j_{12} is the coupling constant between dysprosium moments, and $\hat{H}_{ZEE}$ is Zeeman term. Dy^{3+} moments $\hat{J}_i$ are treated in the $|J,m_J\rangle$ basis sets ($^6H_{15/2}$ multiplet). In this notation, the energy difference between FM and AFM-coupled states of the molecule is $\Delta E_{AFM-FM} = 225j_{12}\cos(\alpha)$, where α is the angle between quantization axes of two Dy^{3+} ions.

The ligand-field parameters for Dy ions were computed *ab initio* at the CASSCF(9,7)/SO-RASSI[16] level for $DyYO@C_{72}$ and $DyYO@C_{74}$ molecules. Given the considerable disorder of experimental structures, DFT-optimized atomic coordinates were used. *Ab initio* calculations showed that Dy^{3+} ions in both clusterfullerenes have easy-axis magnetic anisotropy with the quantization axes aligned along the corresponding Dy–O bonds with a deviation of 2°. In $|J,m_J\rangle$ representation, the four lowest energy Kramers doublets (KDs) are almost pure states with m_J of 15/2 (ground state), 13/2 (near 340 cm^{-1}), 11/2 (near 720 cm^{-1}), and 9/2 (near 1030 cm^{-1}) (Table S9†). Transition probabilities between these states are thus very low (Fig. 5). Further KDs have a more mixed nature, and at higher temperatures the relaxation of magnetization following the Orbach mechanism is expected to proceed *via* the fifth KD at 1180–1200 cm^{-1}, which resembles the situation found experimentally in $Dy_2ScN@C_{80}$ with the Orbach barrier of 1206 ± 15 cm^{-1}.[3e] The overall LF splitting is 1337 cm^{-1} in $Dy_2O@C_{72}$ and 1329 cm^{-1} in $Dy_2O@C_{74}$. In brief, both clusterfullerenes have strongly axial magnetic anisotropy with similar energies and state compositions, and their low-temperature magnetic properties are determined exclusively by the ground state KDs.

The coupling constants j_{12} defining the scale of Dy···Dy interactions are determined by fitting of the experimental magnetization curves to eqn (3) (Fig. S15 and S16†). For $Dy_2O@C_{72}$, the best fit is obtained for the ferromagnetic coupling with $j_{12} = 0.009 \pm 0.002$ cm^{-1}, which gives $\Delta E_{AFM-FM} = 1.5 \pm 0.3$ cm^{-1}. For $Dy_2O@C_{74}$, the optimal j_{12} is less than 0.001 cm^{-1} with the uncertainty of ±0.002 cm^{-1}. The FM and AFM states in $Dy_2O@C_{74}$ are thus degenerate within

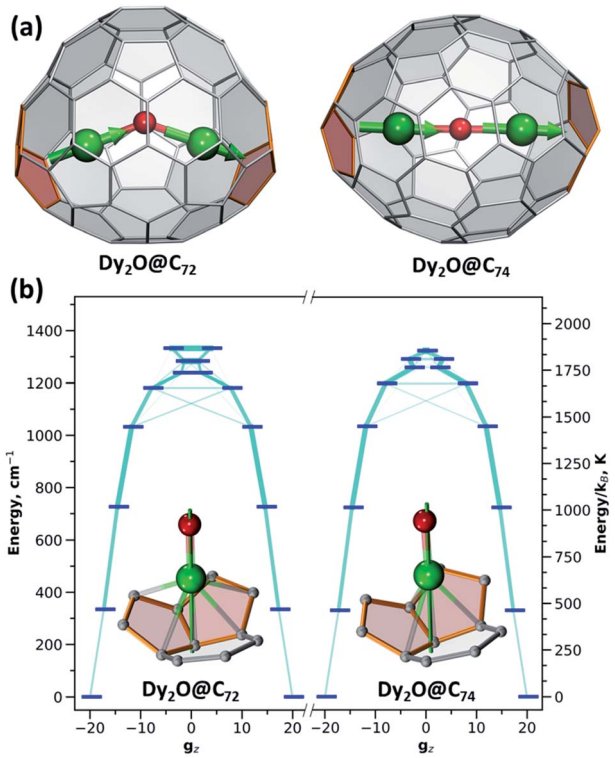

Fig. 5 (a) DFT-optimized molecular structures of $Dy_2O@C_{72}$ and $Dy_2O@C_{74}$ showing alignment of magnetic moment in ferromagnetically-coupled ground-state doublet (Dy is green, O is red, adjacent pentagon pairs are rose; magnetic moments of Dy ions are shown as green arrows). (b) CASSCF/RASSI-computed ligand-field splitting for Dy^{3+} ions in $Dy_2O@C_{72}$ and $Dy_2O@C_{74}$; the thickness of light blue lines corresponds to transition probability. The insets in (b) show Dy-coordinated fragments of the fullerene cage and quantization axis of Dy (green line); Dy–C distances shorter than 2.6 Å are shown as bonds. The scale on the left shows the energy in cm^{-1}, on the right in K.

$|\Delta E_{AFM-FM}| < 0.4\ cm^{-1}$, which means that Dy^{3+} moments are essentially decoupled.

If a magnetic moment of one of the centers in a dinuclear FM-coupled system is flipped, the system arrives in the AFM-coupled state (and *vice versa*). As long as the FM and AFM states have a different energy, the ΔE_{AFM-FM}difference acts as a barrier preventing the QTM, because the latter requires degeneracy of the energy levels. In all dinuclear Dy-clusterfullerenes studied to date the ΔE_{AFM-FM} difference, either positive (FM) or negative (AFM), was large enough to prevent the QTM in zero field. $Dy_2O@C_{74}$ is the first dinuclear Dy-clusterfullerene exhibiting efficient zero-field QTM, which can be explained by the vanishing Dy···Dy coupling. In $Dy_2O@C_{72}$, Dy···Dy coupling is also weak but still sufficient to quench the QTM in zero field.

The Dy···Dy coupling in the Dy_2O clusters found in this work – weak FM in $Dy_2O@C_{72}$ and negligible in $Dy_2O@C_{74}$ – is in a sharp contrast with the situation in $Dy_2O@C_{82}$ isomers, featuring strong AFM coupling with ΔE_{AFM-FM} of (5.4–12.9) cm^{-1}.[7] Such a large variation of the strength of magnetic interactions in seemingly very similar molecules requires a closer look. The overall Dy···Dy coupling in dinuclear spin systems can be divided into exchange and dipolar contributions, ΔE^{exch}_{AFM-FM} and ΔE^{dip}_{AFM-FM}. The latter can be computed exactly when molecular structures and orientations of magnetic moments are known. Using DFT-optimized structures and orientation of quantization axes from *ab initio* calculations, we obtain ΔE^{dip}_{AFM-FM} of 2.99 cm^{-1} in $Dy_2O@C_{72}$ and 2.56 cm^{-1} in $Dy_2O@C_{74}$. Thus, dipolar interactions favour FM arrangement of Dy^{3+} moments and are of the same size as in $Dy_2O@C_{82}$ isomers with ΔE^{dip}_{AFM-FM} of 2.5–3.0 cm^{-1}. Apparently, small overall coupling in $Dy_2O@C_{72,74}$ results from the cancellation of dipolar coupling by exchange interactions, which are therefore antiferromagnetic. To yield the experimentally determined ΔE_{AFM-FM} energies, ΔE^{exch}_{AFM-FM} values should be $-1.5 \pm 0.3\ cm^{-1}$ in $Dy_2O@C_{72}$ and $-2.5 \pm 0.4\ cm^{-1}$ in $Dy_2O@C_{74}$. Thus, it is the antiferromagnetic exchange coupling in the Dy_2O cluster that is changing strongly from one fullerene to another and is therefore responsible for the considerable variation of the magnetic properties in the series of Dy_2O clusterfullerenes. The factors determining exchange interactions in Dy-clusterfullerenes are not very clear yet, and further studies of Dy-oxide clusterfullerenes with different fullerene cages are needed to establish structure–property correlations.

Conclusions

In this work we isolated $Dy_2O@C_s(10528)$–C_{72} and $Dy_2O@C_2(13333)$–C_{74} clusterfullerenes violating the isolated pentagon rule and characterized their structural, electronic, and magnetic properties. The shape of the Dy_2O cluster is determined by the form-factor of the carbon cage and location of pentalene units, leading to the bent cluster in $Dy_2O@C_{72}$ but linear one in $Dy_2O@C_{74}$. Both fullerenes are single molecule magnets showing hysteresis up to 7 K in $Dy_2O@C_{72}$ and 14 K in $Dy_2O@C_{74}$, the latter being the highest temperature among Dy-clusterfullerenes. The magnetic Dy···Dy interactions in Dy_2O clusters are characterized by the ferromagnetic dipolar coupling counterbalanced by the antiferromagnetic exchange. In $Dy_2O@C_{74}$, these two contributions cancel each other completely leading to decoupled Dy moments and zero-field quantum tunnelling of magnetization. As a result, magnetization of $Dy_2O@C_{74}$ relaxes fast in zero field, but the relaxation becomes slow once the tunnelling is quenched in a finite magnetic field. This study demonstrates that the shape flexibility of the Dy_2O cluster and its conformity with the fullerene form-factor is reflected in the substantial variation of the Dy_2O-clusterfullerene magnetic properties with the carbon cage. This cage-adaptive SMM behaviour suggests that even stronger variability of magnetic properties may be achieved in future exploration of lanthanide-oxide clusterfullerenes with different carbon cages.

Conflicts of interest

There are no conflicts to declare.

Acknowledgements

G. Velkos and W. Yang contributed equally to this work. The authors acknowledge funding from the European Union's Horizon 2020 research and innovation programme, European Research Council (grant agreement No. 648295 to A. A. P.), and Marie Skłodowska-Curie action (grant agreement No. 748635 to S. M. A.), and the Deutsche Forschungsgemeinschaft (grants PO 1602/4-1 and 1602/5-1 to A. A. P.). C. N. thanks the National Science Foundation China (NSFC 91961109, 51302178), the NSF of Jiangsu Province (BK20171211), Priority Academic Program Development of Jiangsu Higher Education Institutions (PAPD) and the project of scientific and technologic infrastructure of Suzhou (SZS201708). Computational resources were provided by the Center for High Performance Computing at the TU Dresden. We appreciate the help from Dr Anja U. B. Wolter and Sebastian Gaβ in magnetic measurements and technical support with computational resources in IFW Dresden by Ulrike Nitzsche.

Notes and references

§ Crystals were grown by layering the benzene solution of nickel octaethylporphyrin (Ni(OEP)) onto the CS_2 solution of the $Dy_2O@C_{2n}$ ($2n = 72, 74$) isomers. The as-prepared crystals $Dy_2O@C_s(10528)$–$C_{72}\cdot Ni(OEP)\cdot 2(C_6H_6)$ and $Dy_2O@C_2(13333)$–$C_{74}\cdot Ni(OEP)\cdot C_6H_6\cdot CS_2$ were measured with Bruker APEX II at 120 and 173 K, respectively. The structures were solved using direct methods[17] and refined on F2 using full-matrix least-squares using the SHELXL2015 crystallographic software package.[18] Hydrogen atoms were inserted at calculated positions and constrained with isotropic thermal parameters. The crystal data are presented in Table S1.† The data can be obtained free of charge from the Cambridge Crystallographic Data Centre with CCDC no. 1974305 and 1974314,† respectively.

1 (*a*) S. Yang, T. Wei and F. Jin, *Chem. Soc. Rev.*, 2017, **46**, 5005; (*b*) A. A. Popov, *Endohedral Fullerenes: Electron Transfer and Spin*, Springer International Publishing, Cham, 2017; (*c*) A. A. Popov, S. Yang and L. Dunsch, *Chem. Rev.*, 2013, **113**, 5989; (*d*) X. Lu, W. Shen and S. Hu, *Chem.–Eur. J.*, 2020, DOI: 10.1002/chem.201905306.

2 (*a*) F. Liu, S. Wang, C.-L. Gao, Q. Deng, X. Zhu, A. Kostanyan, R. Westerström, F. Jin, S.-Y. Xie, A. A. Popov, T. Greber and S. Yang, *Angew. Chem., Int. Ed.*, 2017, **56**, 1830; (*b*) F. Liu, C.-L. Gao, Q. Deng, X. Zhu, A. Kostanyan, R. Westerström, S. Wang, Y.-Z. Tan, J. Tao, S.-Y. Xie, A. A. Popov, T. Greber, *et al.*, *J. Am. Chem. Soc.*, 2016, **138**, 14764; (*c*) R. Westerström, J. Dreiser, C. Piamonteze, M. Muntwiler, S. Weyeneth, K. Krämer, S.-X. Liu, S. Decurtins, A. Popov, S. Yang, L. Dunsch and T. Greber, *Phys. Rev. B: Condens. Matter Mater. Phys.*, 2014, **89**, 060406; (*d*) J. Dreiser, R. Westerström, Y. Zhang, A. A. Popov, L. Dunsch, K. Krämer, S.-X. Liu, S. Decurtins and T. Greber, *Chem.–Eur. J.*, 2014, **20**, 13536; (*e*) R. Westerström, J. Dreiser, C. Piamonteze, M. Muntwiler, S. Weyeneth, H. Brune, S. Rusponi, F. Nolting, A. Popov, S. Yang, L. Dunsch and T. Greber, *J. Am. Chem. Soc.*, 2012, **134**, 9840; (*f*) T. Wang and C. Wang, *Small*, 2019, **15**, 1901522; (*g*) M. Nie, J. Xiong, C. Zhao, H. Meng, K. Zhang, Y. Han, J. Li, B. Wang, L. Feng, C. Wang and T. Wang, *Nano Res.*, 2019, **12**, 1727.

3 (*a*) L. Spree and A. A. Popov, *Dalton Trans.*, 2019, **48**, 2861; (*b*) D. Krylov, F. Liu, A. Brandenburg, L. Spree, V. Bon, S. Kaskel, A. Wolter, B. Buchner, S. Avdoshenko and A. A. Popov, *Phys. Chem. Chem. Phys.*, 2018, **20**, 11656; (*c*) C. H. Chen, D. S. Krylov, S. M. Avdoshenko, F. Liu, L. Spree, R. Westerström, C. Bulbucan, M. Studniarek, J. Dreiser, A. U. B. Wolter, B. Büchner and A. A. Popov, *Nanoscale*, 2018, **10**, 11287; (*d*) C. Schlesier, L. Spree, A. Kostanyan, R. Westerström, A. Brandenburg, A. U. B. Wolter, S. Yang, T. Greber and A. A. Popov, *Chem. Commun.*, 2018, **54**, 9730; (*e*) D. S. Krylov, F. Liu, S. M. Avdoshenko, L. Spree, B. Weise, A. Waske, A. U. B. Wolter, B. Büchner and A. A. Popov, *Chem. Commun.*, 2017, **53**, 7901; (*f*) F. Liu, D. S. Krylov, L. Spree, S. M. Avdoshenko, N. A. Samoylova, M. Rosenkranz, A. Kostanyan, T. Greber, A. U. B. Wolter, B. Büchner and A. A. Popov, *Nat. Commun.*, 2017, **8**, 16098; (*g*) C.-H. Chen, D. S. Krylov, S. M. Avdoshenko, F. Liu, L. Spree, R. Yadav, A. Alvertis, L. Hozoi, K. Nenkov, A. Kostanyan, T. Greber, A. U. B. Wolter, *et al.*, *Chem. Sci.*, 2017, **8**, 6451; (*h*) T. Greber, A. P. Seitsonen, A. Hemmi, J. Dreiser, R. Stania, F. Matsui, M. Muntwiler, A. A. Popov and R. Westerström, *Phys. Rev. Mater.*, 2019, **3**, 014409; (*i*) K. Junghans, C. Schlesier, A. Kostanyan, N. A. Samoylova, Q. Deng, M. Rosenkranz, S. Schiemenz, R. Westerström, T. Greber, B. Büchner and A. A. Popov, *Angew. Chem., Int. Ed.*, 2015, **54**, 13411; (*j*) R. Westerström, A.-C. Uldry, R. Stania, J. Dreiser, C. Piamonteze, M. Muntwiler, F. Matsui, S. Rusponi, H. Brune, S. Yang, A. Popov, B. Büchner, *et al.*, *Phys. Rev. Lett.*, 2015, **114**, 087201; (*k*) A. Brandenburg, D. S. Krylov, A. Beger, A. U. B. Wolter, B. Büchner and A. A. Popov, *Chem. Commun.*, 2018, **54**, 10683.

4 (*a*) K. L. M. Harriman, D. Errulat and M. Murugesu, *Trends in Chemistry*, 2019, **1**, 425; (*b*) A. K. Bar, P. Kalita, M. K. Singh, G. Rajaraman and V. Chandrasekhar, *Coord. Chem. Rev.*, 2018, **367**, 163; (*c*) B. M. Day, F.-S. Guo and R. A. Layfield, *Acc. Chem. Res.*, 2018, **51**, 1880; (*d*) J.-L. Liu, Y.-C. Chen and M.-L. Tong, *Chem. Soc. Rev.*, 2018, **47**, 2431; (*e*) Z. Zhu, M. Guo, X.-L. Li and J. Tang, *Coord. Chem. Rev.*, 2019, **378**, 350; (*f*) J. Dreiser, *J. Phys.: Condens. Matter*, 2015, **27**, 183203; (*g*) S. T. Liddle and J. van Slageren, *Chem. Soc. Rev.*, 2015, **44**, 6655; (*h*) J. Luzon and R. Sessoli, *Dalton Trans.*, 2012, **41**, 13556; (*i*) D. N. Woodruff, R. E. P. Winpenny and R. A. Layfield, *Chem. Rev.*, 2013, **113**, 5110; (*j*) C. A. P. Goodwin, F. Ortu, D. Reta, N. F. Chilton and D. P. Mills, *Nature*, 2017, **548**, 439; (*k*) F.-S. Guo, B. M. Day, Y.-C. Chen, M.-L. Tong, A. Mansikkamäki and R. A. Layfield, *Science*, 2018, **362**, 1400; (*l*) K. R. McClain, C. A. Gould, K. Chakarawet, S. Teat, T. J. Groshens, J. R. Long and B. G. Harvey, *Chem. Sci.*, 2018, **9**, 8492; (*m*) C. Gould, K. R. McClain, J. Yu, T. J. Groshens, F. Furche, B. G. Harvey and J. R. Long, *J. Am. Chem. Soc.*, 2019, **141**, 12967; (*n*) F. Liu, G. Velkos, D. S. Krylov, L. Spree, M. Zalibera, R. Ray, N. A. Samoylova, C.-H. Chen, M. Rosenkranz, S. Schiemenz, F. Ziegs,

K. Nenkov, *et al.*, *Nat. Commun.*, 2019, **10**, 571; (*o*) G. Velkos, D. Krylov, K. Kirkpatrick, L. Spree, V. Dubrovin, B. Büchner, S. Avdoshenko, V. Bezmelnitsyn, S. Davis, P. Faust, J. Duchamp, H. Dorn, *et al.*, *Angew. Chem., Int. Ed.*, 2019, **58**, 5891; (*p*) F. Liu, L. Spree, D. S. Krylov, G. Velkos, S. M. Avdoshenko and A. A. Popov, *Acc. Chem. Res.*, 2019, **52**, 2981.

5 (*a*) L. Abella, Y. Wang, A. Rodríguez-Fortea, N. Chen and J. M. Poblet, *Inorg. Chim. Acta*, 2017, **468**, 91; (*b*) L. Feng, Y. Hao, A. Liu and Z. Slanina, *Acc. Chem. Res.*, 2019, **52**, 1802; (*c*) A. Liu, M. Nie, Y. Hao, Y. Yang, T. Wang, Z. Slanina, H. Cong, L. Feng, C. Wang and F. Uhlik, *Inorg. Chem.*, 2019, **58**, 4774; (*d*) H. Cong, A. Liu, Y. Hao, L. Feng, Z. Slanina and F. Uhlik, *Inorg. Chem.*, 2019, **58**, 10905; (*e*) Q. Tang, L. Abella, Y. Hao, X. Li, Y. Wan, A. Rodríguez-Fortea, J. M. Poblet, L. Feng and N. Chen, *Inorg. Chem.*, 2016, **55**, 1926; (*f*) Y. Hao, Q. Tang, X. Li, M. Zhang, Y. Wan, L. Feng, N. Chen, Z. Slanina, L. Adamowicz and F. Uhlík, *Inorg. Chem.*, 2016, **55**, 11354; (*g*) T. Yang, Y. Hao, L. Abella, Q. Tang, X. Li, Y. Wan, A. Rodríguez-Fortea, J. M. Poblet, L. Feng and N. Chen, *Chem.–Eur. J.*, 2015, **21**, 11110; (*h*) Q. Tang, L. Abella, Y. Hao, X. Li, Y. Wan, A. Rodríguez-Fortea, J. M. Poblet, L. Feng and N. Chen, *Inorg. Chem.*, 2015, **54**, 9845; (*i*) M. Zhang, Y. Hao, X. Li, L. Feng, T. Yang, Y. Wan, N. Chen, Z. Slanina, F. Uhlik and H. Cong, *J. Phys. Chem. C*, 2014, **118**, 28883; (*j*) B. Q. Mercado, M. A. Stuart, M. A. Mackey, J. E. Pickens, B. S. Confait, S. Stevenson, M. L. Easterling, R. Valencia, A. Rodriguez-Fortea, J. M. Poblet, M. M. Olmstead and A. L. Balch, *J. Am. Chem. Soc.*, 2010, **132**, 12098.

6 M. K. Singh and G. Rajaraman, *Chem. Commun.*, 2016, **52**, 14047.

7 W. Yang, G. Velkos, F. Liu, S. M. Sudarkova, Y. Wang, J. Zhuang, H. Zhang, X. Li, X. Zhang, B. Büchner, S. M. Avdoshenko, A. A. Popov, *et al.*, *Adv. Sci.*, 2019, **6**, 1901352.

8 N. Chen, C. M. Beavers, M. Mulet-Gas, A. Rodriguez-Fortea, E. J. Munoz, Y.-Y. Li, M. M. Olmstead, A. L. Balch, J. M. Poblet and L. Echegoyen, *J. Am. Chem. Soc.*, 2012, **134**, 7851.

9 Y. Feng, T. Wang, J. Wu, L. Feng, J. Xiang, Y. Ma, Z. Zhang, L. Jiang, C. Shu and C. Wang, *Nanoscale*, 2013, **5**, 6704.

10 P. Zhao, X. Zhao and M. Ehara, *Inorg. Chem.*, 2017, **56**, 10195.

11 (*a*) J. Hafner, *J. Comput. Chem.*, 2008, **29**, 2044; (*b*) G. Kresse and J. Hafner, *Phys. Rev. B: Condens. Matter Mater. Phys.*, 1993, **47**, 558; (*c*) G. Kresse and D. Joubert, *Phys. Rev. B: Condens. Matter Mater. Phys.*, 1999, **59**, 1758; (*d*) J. P. Perdew, K. Burke and M. Ernzerhof, *Phys. Rev. Lett.*, 1996, **77**, 3865; (*e*) S. Grimme, *Wiley Interdiscip. Rev.: Comput. Mol. Sci.*, 2011, **1**, 211.

12 M. Murrie, A. Canaj, S. Dey, O. Cespedes, C. Wilson and G. Rajaraman, *Chem. Commun.*, 2020, **56**, 1533.

13 D. Gatteschi, R. Sessoli and J. Villain, *Molecular Nanomagnets*, Oxford University Press, New York, 2006.

14 A. Singh and K. N. Shrivastava, *Phys. Status Solidi B*, 1979, **95**, 273.

15 N. F. Chilton, R. P. Anderson, L. D. Turner, A. Soncini and K. S. Murray, *J. Comput. Chem.*, 2013, **34**, 1164.

16 (*a*) F. Aquilante, J. Autschbach, R. K. Carlson, L. F. Chibotaru, M. G. Delcey, L. De Vico, I. F. Galván, N. Ferré, L. M. Frutos, L. Gagliardi, M. Garavelli, A. Giussani, *et al.*, *J. Comput. Chem.*, 2016, **37**, 506; (*b*) L. F. Chibotaru and L. Ungur, *J. Chem. Phys.*, 2012, **137**, 064112.

17 O. V. Dolomanov, L. J. Bourhis, R. J. Gildea, J. A. Howard and H. Puschmann, *J. Appl. Crystallogr.*, 2009, **42**, 339.

18 G. M. Sheldrick, *Acta Crystallogr., Sect. C: Struct. Chem.*, 2015, **71**, 3.

